Journal of Materials Chemistry B

Accepted Manuscript

ROYAL SOCIETY OF CHEMISTRY

www.rsc.org/materialsB

Anti-biofouling Surface with Sub-20 nm Heterogeneous Nanopatterns

Lei Shen[a,*], *Jun Xie*[a, b], *Juan Tao*[b,*] and *Jintao Zhu*[a,*]

[a]School of Chemistry and Chemical Engineering, Huazhong University of Science and Technology (HUST), Wuhan, 430074, China. Email: lshen@hust.edu.cn, jtzhu@mail.hust.edu.cn.
[b]Department of Dermatology, Affiliated Union Hospital, Tongji Medical College, HUST, Wuhan, 430022, China. Email: tjhappy@126.com.

†Electronic supplementary information (ESI) available: The SPR results showing lysozome adsorption on PS_{60}-*b*-$PHEMA_{150}$ nanopatterns at 25 and 40 ^{o}C; Optical microscopy images showing A375 and DU145 cell behaviors on four polymer thin films.

ABSTRACT: We develop a novel heterogeneous pattern with nanometer-sized spots surrounded with a bio-inert matrix by using diblock copolymer thin film. The nanopattern with features down to 20 nm is highly resistant to protein adsorption and cell adhesion. By providing the domelike topography similar to biology relevant size, such heterogeneous nanopattern demonstrates an excellent anti-biofouling property to control over the protein-surface and cell-surface interactions at the molecular level.

Introduction

The platform with heterogeneous patterns is the cornerstone of various biology equipments, such as protein microarray chips, cell incubation substrates and drug screening devices. Specifically, the patterns with physical dimensions of 100 nm or less, a size range relative to protein molecules and the footprints of cells, are required to provide as a potential template for fundamentally studying the protein-surface and cell-surface interactions at the molecular level.[1] Block copolymers (BCP), with two immiscible blocks covalently linked together, can microphase-separate into nanometer-sized periodic domains with inherently high spot density when casted as a thin film[2,3] and it is thus widely explored as the template to pattern proteins and/or to study the response of living cells to the nanostructures. For example, poly(styrene)-*block*-poly(methyl methacrylate) (PS-*b*-PMMA)[4,5], PS-*block*-poly(4-vinylpyridine) (PS-*b*-PVP) [6,7] and PS-*block*-poly(isoprene) (PS-*b*-PI)[8] BCP films have been developed to pattern proteins. Besides these BCP films, the nanostructured PS-*b*-(fluorinated-PS) thin film has also been utilized to study the cell adhesion towards surfaces.[9] Recently, PS-*block*-poly(ethylene glycol) (PS-*b*-PEG) thin film with 25-nm-sized PEG features surrounded with a PS matrix are generated to elucidate the interactions between cells and surfaces.[10] More examples about the nano-scaled bioarray patterns by BCP thin films can be found in a recent review paper.[11]

Yet, one significant issue was ignored in the previous reports. Generally, surface property for bioarray pattern fabrication should satisfy the following key criteria: the surface is inherently inert and resists the nonspecific protein adsorption to retain the native conformation and bio-activity of immobilized proteins or cell tissues; that is, the resulting nanometer-sized protein-binding regions should be introduced into a protein-resistant surface. As the material preferred to being used in the previous works, PS matrix is rigid and can stabilize the whole surface feature under aqueous environment, but it is hydrophobic with high surface energy so that proteins can

easily adsorb on it and denature through the long-range hydrophobic interaction.[12] As the other block of the BCPs, PMMA, PVP and PI are also attractive to proteins.[13,14] Some BCP surfaces with different domain sizes have been demonstrated to have the ability to decrease thrombogenicity and control the blood platelet formation near the surface.[15] But, in these reports, the separated domain areas are much larger than hundreds of nanometer which exceed the size of proteins. Therefore, one big challenge is how to develop robust nanopatterns surrounded with a bio-inert matrix with strong resistance to protein adsorption for potentially excellent application in next generation of lab-on-a-chip.

Herein, we developed patterns down to 20 nm range by using PS-*block*-poly(2-hydroxyethyl methacrylate) (PS-*b*-PHEMA) BCP thin film with PHEMA as the majority phase. Generally, PHEMA is water-soluble at low molecular weight due to its pendant hydroxyl group, but not as hydrophilic as PEG.[16] While, when the number of repeat HEMA unit is more than 50, PHEMA is water-insoluble but still retains its biocompatibility. This is one of the reasons that PHEMA is commonly used in applications such as contact lenses and implant materials.[17] As a consequence, PHEMA is an ideally optimal matrix candidate for nanopattern design. PS is chosen as the minority domain for easily introducing functional groups for protein immobilization and cell screening in future work. In this paper, we evaluate the protein adsorption and cell adhesion on PS-*b*-PHEMA BCP thin films with various morphologies by varying the block ratio of the BCPs. The objective of this work is to develop the heterogeneous nanopatterns down to 20 nm size with super-low bio-fouling property. We, for the first time, generated a robust nanopattern with similar size to protein molecules or the footprints of cells surrounded with a bio-inert matrix. By preventing the non-specific protein adsorption and cell adhesion, such nanopattern can be utilized in a wide range of bio-applications instead of traditional PS-matrix based templates.

Materials and methods

Materials. PS_{200}-*b*-$PHEMA_{50}$ (polydispersity index (PDI) = 1.10, subscript is the number of repeating units of each block), PS_{60}-*b*-$PHEMA_{150}$ (PDI = 1.18), PS_{140}-*b*-$PHEMA_{150}$ (PDI = 1.15) diblock copolymers and PS_{200} (PDI = 1.04) were obtained from Polymer Source, Inc (Canada) and used as received. $PHEMA_{7700}$ was obtained from Sigma-Aldrich. All solvents used were reagent grade and obtained from Shanghai Chemical Reagent Inc. (China). Four proteins, white egg lysozome (LYS), fibrinogen from human plasma (FBN), albumin from bovine serum (BSA) and myoglobin from equine skeletal muscle (MYO), were purchased from Sigma-Aldrich (purity ≥ 98%). Phosphate buffered saline (PBS) was freshly prepared from sodium and potassium salts: NaCl (80 g), KCl (2 g), Na_2HPO_4 (2 g) and KH_2PO_4 (6.5 g) were dissolved in 1 liter of deionized water to give a solution of pH 7.4 at 25 ^oC. Protein solutions in the concentration range of 5-50 μg/mL were prepared in PBS buffer immediately before use.

Preparation of polymer thin films. PS_{200}-*b*-$PHEMA_{50}$ (1.0 wt%) was firstly dissolved in $CHCl_3$, while PS_{60}-*b*-$PHEMA_{150}$ (1.0 wt%) and PS_{140}-*b*-$PHEMA_{150}$ (1.0 wt%) were dissolved in $CHCl_3$/methanol mixed solvent (9:1 v:v). Each polymer thin film was generated through spin-coating the polymer solution on a freshly prepared glass-coated gold substrate at 3000 rmp for 60s. To facilitate polymer chain rearrangement into microphase separation, the pre-cast polymer thin film was annealed in $CHCl_3$/DMF (1:1 v:v) vapor for 3h.

Surface morphology of the polymer thin films was imaged on an AFM (Agilent Technologies 5500) in the AC mode. A silicon cantilever-mounted tip (10 nm radius of curvature, 42 N/m spring constant; 300 kHz resonance frequency) was used in all experiments.

The chemical components at the surfaces of the polymer thin films were recorded by X-ray photoelectron (XPS) technique. All XPS measurements were carried out on a Kratos AXIS Ultra

DLD model with an Al K_α X-ray anode at an analyzer pass energy of 80 eV. The total data acquisition time for each spectrum was approximate 2.5 min.

Protein adsorption. Protein adsorption experiments were carried out on a commercial surface plasma resonance instrument (SPRImager II, GWC Technologies Inc., Madison, WI). The surface plasmon was excited by collimated polychromatic *p*-polarized light directed at a gold film sample through a prism assembly at an angle of incidence θ. The intensity change (ΔI) measured at a constant angle is directly proportional to the change in the bulk refractive index of the solution near the sensor surface. The effective thickness (d) for the adsorbed layer is given by $d = (l_d / 2)[\Delta I / s(n_a - n_s)]$ where l_d is the decay length of the evanescent field near the gold surface (typically 37% of the wavelength of the light); s is a calibrated sensitivity parameter for the instrument; and n_s = 1.334 is the refractive index of the solution. The parameter s was calibrated by a 1% ethanol/ H_2O mixture. Based on the effective thickness determined in the experiment, we can estimate the surface coverage (C) of adsorbed molecules as: C (molecules/cm^2) = d/V, where V is the specific volume (cm^3/g) of the protein in the solution. The dimensions of the fluidic channel and the flow rate (3 μL/s) correspond to Lamellar flow.

Cell adhesion. Cell adhesion experiments were performed by using three different adherent cells, murine fibroblast cells NIH-3T3 (Wuhan Boster Biological Engineering CO., Ltd.), human melanoma cells A375 and human prostate cancer cells DU145 (gifted from professor G. X. Shen, Department of immunology, Tongji medical college, HUST) on BCP coated cover glass in 6-well plates. 1 × 10^6 cells/well were grown in 1.5 mL cell medium (high glucose DMEM with 10% fetal calf serum, HyClone, Logan, USA) and incubated with BCP coated cover glass in a 100% humidified incubator at 37 ℃ with 5% CO_2 for 24 hrs. Cell morphologies were observed under a commercial optical microscope (Olympus Optical Co. LTD. IX71S1F-2, Tokyo, Japan).

For FM characterization, cells on BCP coated cover glass were stained as follows. First, the cover glass was rinsed by PBS to remove non-adherent cells. The remaining cells were fixed with 4% 500 μL paraformaldehyde (G1101, Goodbio technology CO., Ltd.) for 20 min. After washing with PBS, the cells were permeabilized with 100 μL rupture working solution (0.5% Triton ×100, MSDS 0694, AMRESCO LLC., Solon, USA) for 30 min at room temperature, then rinsed with PBS again. Second, F-actin and microtubules were stained with a combination of green fluorescence dye FITC labeled Phalloidin and β-tublin (G1028 and GB11005, Goodbio technology CO., Ltd.), respectively. Together with the above solution containing fluorescence dyes, cells were incubated in the dark environment at 4 ℃ overnight. After rinsed with PBS, 100 μL red fluorescence dye CY3 labeled goat anti-rabbit secondary antibody (GB21303, Goodbio technology CO., Ltd.) was added and cells were incubated in the dark at 4 ℃ again for 10 min. After rinsed with PBS, cells were stained with 100μL 4,6-diamidino-2-phenylindole (DAPI, G1012, Goodbio technology CO., Ltd.) for 5 min followed by PBS rinsing again. In this case, F-actin, microtubules and nuclei were labeled with green, red and blue fluorescence signal, respectively. Subsequently, the cover glass with adherent cells was mounted with anti-fluorescein quencher (G1401, Goodbio technology CO., Ltd.) for FM characterization. Fluorescence microscope (Nikon, TE2000, Tokyo, Japan) was used to assess the extent of cell adhesion.

Results and discussion

To prepare the heterogeneous nano-patterns with different morphologies, we chose three types of PS-*b*-PHEMA diblock copolymers: PS_{60}-*b*-$PHEMA_{150}$, PS_{140}-*b*-$PHEMA_{150}$ and PS_{200}-*b*-$PHEMA_{50}$ which can self-assemble into periodic nano-patterns: PS cylinder (diameter ~ 20 nm) in PHEMA matrix, lying-down PS-*b*-PHEMA lamella (width ~ 20 nm) and PHEMA cylinder (diameter ~ 15 nm) in PS matrix, respectively, as shown by dry state AFM technique in **Fig. 1**. The PS and PHEMA content at the surfaces of heterogeneous PS-*b*-PHEMA nano-patterns were

determined by high resolution C 1s XPS spectra as shown in **Fig. 2**. In this method, the C 1s peak of PHEMA consists of three different carbons and it is divided into three Gaussian peaks with binding energy of 285.0, 286.7, and 288.9 eV, which corresponds to C–C, C–C–O, and O=C–O, respectively. The PHEMA content at the surfaces was calculated from the percentage of O=C–O (288.9 eV) peak against the total carbon atoms. The mole ratios of PS:PHEMA at the surfaces of PS_{60}-*b*-$PHEMA_{150}$, PS_{140}-*b*-$PHEMA_{150}$ and PS_{200}-*b*-$PHEMA_{50}$ nano-patterns were calculated as 0.4:1, 2:1, and 6:1, respectively, demonstrating the chemical components variation of these heterogeneous surfaces.

It is demonstrated by liquid state AFM characterization that these PS-*b*-PHEMA nanopatterns keep their original features and the whole films are stable without apparent swelling in water for at least 24 h. The result is consistent with the insolubility of PHEMA at higher molecular weight near neutral pH value. Usually, neat PHEMA film does partially swell in aqueous solution, while the presence of PS cylinder domains in PS_{60}-*b*-$PHEMA_{150}$ nanopattern prevents the swelling of PHEMA matrix. Notably, PS-*b*-PEG thin film is not an appropriate template for the fabrication of protein repulsive nanopattern since the film swells and the patterns destruct in aqueous phase even when PEG is the minority cylinders.[18] In control experiments, we prepared $PHEMA_{7700}$ and PS_{200} homogeneous surfaces by directly casting their chloroform solutions onto glass substrate. In any case mentioned above, the casted films present low surface roughness values (rms<1 nm) on the micrometer scale.

Nonspecific protein adsorption on the five above-mentioned polymer nanopatterns was probed by using SPR technique. SPR gold sensor coated with desirable polymer nanopatterns was equilibrated before measurement by washing with PBS buffer solution and then switched to protein PBS solution. After the adsorption experiment, the gold sensor was finally switched back to PBS buffer again to wash the weakly bond protein away and stop the protein adsorption

process. From the increase of SPR signal, the amount of protein irreversibly adsorbed on polymer films was quantitatively calculated. First, the protein adsorption experiments were performed by choosing lysozome, a small protein molecule (M_w ~ 14 kDa, pI = 11.1) with strongly positively charged in neutral pH buffer solution. **Fig. 3** summarizes the amount of lysozome nonspecifically adsorbed on $PHEMA_{7700}$, PS_{60}-*b*-$PHEMA_{150}$, PS_{140}-*b*-$PHEMA_{150}$, PS_{200}-*b*-$PHEMA_{50}$ and PS_{200} thin films. Our result indicates that lysozome adsorbs strongly on PS while less on PHEMA homopolymer film, which is consistent with previous protein adsorption experiments where hydrophilic PHEMA is more resistant to proteins than hydrophobic PS.[19] On PS-*b*-PHEMA thin films, the amount of lysozome adsorption decreases with the increase of PHEMA composition. Interestingly, there is almost no lysozome adsorption occurring on PS_{60}-*b*-$PHEMA_{150}$, indicating that the feature with 20 nm sized PS domelike domains surrounded with a PHEMA matrix provides strong resistance to lysozome. To further confirm the protein-repulsive property of PS_{60}-*b*-$PHEMA_{150}$ nanopatterns, we investigate the adsorption of other three different protein models (fibrinogen from human plasma (FBN) (M_w ~ 130 kDa), albumin from bovine serum (BSA) (M_w ~ 67kDa) and myoglobin from equine skeletal muscle (MYO) (M_w ~ 17kDa)) on this thin film. FBN and BSA are the typical "soft" proteins with low level of structure stability, while MYO is "hard" one with high level of stability. Clearly, the SPR signals behave as no detectable change before and after protein adsorption at different concentrations, further indicating that PS_{60}-*b*-$PHEMA_{150}$ nanopattern is super resistant to protein molecules (**Fig. 4**). Notably, such PS_{60}-*b*-$PHEMA_{150}$ nanopattern retains inert to proteins above human body temperature (**Fig. S1**, †ESI), which demonstrates more advantages than grafted PEG brush, one of the well-known protein resistant material but loosing anti-biofouling property above 35 ^{o}C.[20] The above results demonstrate that PS_{60}-*b*-$PHEMA_{150}$ nano-patterns provide super resistance to proteins and such patterns are robust and retain the inert property at both room and higher temperatures.

It is worth noting that only the reduction of protein adsorption is insufficient evidence for anti-biofouling property. As the basic function unit of organism, cell usually adheres to substrate through the outer membrane proteins and carbohydrates on cell surface, and eventually grows into large area of bio-infection layers on substrate.[21,22] Thus, it is well accepted that reduction of protein adsorption results in a reduction of cell adhesion and spreading. To investigate the cell adhesion on PS-*b*-PHEMA nano-patterns, we choose the typical adherent cell, murine fibroblast cells NIH-3T3, which is the most common cell of connective tissue in animals and adheres to bio-interface to synthesize extracellular matrix and collagen.[23] **Fig. 5** shows the behavior of fibroblast cells on four aforementioned substrates after 24 h of cultivation. A large number of fibroblast cells are fully stretched and highly spread on PS and PS_{200}-*b*-$PHEMA_{50}$ (**Fig. 5a** and **5b**). With the increase of PHEMA component on PS_{140}-*b*-$PHEMA_{150}$ (**Fig. 5c**), fibroblast cells are observed as elongated morphology with less-spread area. On PS_{60}-*b*-$PHEMA_{150}$ (**Fig. 5d**), very few fibroblast cell adheres to substrate and most of cells pretend to aggregate as globular form in solution, implying that such PS_{60}-*b*-$PHEMA_{150}$ template strongly resists cell adhesion. To further confirm the cell-repulsive property of PS_{60}-*b*-$PHEMA_{150}$ nanopatterns, we also carry out adhesion study by using two other types of adherent cells, human prostate carcinoma DU145 and human melanoma cell A375, which require necessary attachment onto extracellular substrate to survive and proliferate. Clearly, DU145 cells attach to and proliferate well on PS (**Fig. 6a**). However, on PS_{200}-*b*-$PHEMA_{50}$ and PS_{140}-*b*-$PHEMA_{150}$ with more PHEMA component, DU145 cells adhere to surface with less-spread area (**Fig. 6b** and **6c**). DU145 cells cannot stick to PS_{60}-*b*-$PHEMA_{150}$ substrate and maintain the stable globular form after the cultivation for 24 h (**Fig. 6d**). Optical microscopy images (**Fig. S2** and **S3**, †ESI) show that both DU145 and A375 cells aggregate and lose their initial native morphology in buffer solution, which indirectly proves that there is no interaction between PS_{60}-*b*-$PHEMA_{150}$ surface and adherent cells. Taken together,

above cell adhesion experiments demonstrate that PS_{60}-*b*-$PHEMA_{150}$ template with 20 nm-sized PS domains surrounded with a PHEMA matrix strongly resists cell adhesion in culture medium.

Heterogeneous surfaces with mixed or patterned hydrophobic/hydrophilic microdomains have been developed for inhibiting bio-adhesion. By lowing surface energy, the heterogeneous surface can exhibit highly resistant to biomolecules, partially according to wetting theory. For example, silicone-urethane coatings [24] and PEG-fluorinated strips [25] were fabricated for bio-organism adhesion experiments. Although these micro-structured domains had the lowest barnacle and zoospore adsorption, the dimensions of these domains were micrometer scale which is much larger than that of protein molecules. Thus, this template is not suitable for individual protein immobilization. Additionally, polymer networks consist of hyper-branched fluoro-polymers and PEG chains (HBFP-PEG) were observed to phase-separate into smaller compositional structures, resulting in highest resistance toward protein adsorption.[26,27] Yet, the surface morphologies reconstructed due to the highly preferential of PEG to water molecules when placed the surface in aqueous environment. Thus, the development of robust anti-fouling patterns with nanometer sized protein-binding regions is highly desirable. Generally, PHEMA has been demonstrated to be able to minimize protein adsorption, but not as efficient as PEG in protein repellency at room temperature. In the case of PS_{60}-*b*-$PHEMA_{150}$, heterogeneous nanopatterns with highly ordered PS domains surrounded with a PHEMA matrix are a better option to obtain excellent anti-fouling behavior. To evaluate the surface energy of PS-*b*-PHEMA surfaces based on traditional wetting theory, we carry out the measurement of liquid-solid contact angle to evaluate solid surface tension (γ_S) by using two liquids (water and hexadecane) with known surface tensions. The γ_S of PS-*b*-PHEMA films are extracted from the measured contact angle (θ) based on the well-known Young's equation as:

$$\gamma_L\left(1+\cos\theta\right)=2\left[\left(\gamma_S^D\gamma_L^D\right)^{1/2}+\left(\gamma_S^P\gamma_L^P\right)^{1/2}\right] \qquad (1)$$

where $\gamma_S=\gamma_S^D+\gamma_S^P$, the γ_S^D and γ_S^P are the dispersion and dipole-dipole components of surface tension. The static contact angles of water (θ_w) on PS, PS_{200}-*b*-$PHEMA_{50}$, PS_{140}-*b*-$PHEMA_{150}$, PS_{60}-*b*-$PHEMA_{150}$ and PHEMA are 102 $\pm 2^o$, 92 $\pm 2^o$, 67 $\pm 2^o$, 62 $\pm 2^o$ and 55 $\pm 2^o$, respectively, which have been well characterized in our previous report.[28] With the increase of PHEMA component, these films exhibit continuously increased surface tensions from γ_{PS} = 32.1 mN/m to $\gamma_{PS60\text{-}b\text{-}PHEMA150}$ = 46.6 mN/m, with no such lowest surface energy as the cases of silicone-urethane coating[24] and HBFP-PEG template[26, 27]. Based on the traditional wetting theory, proteins actually adhere to PS_{60}-*b*-$PHEMA_{150}$, in contradiction to the observed reduction in protein binding. Obviously, our case cannot be simply explained by traditional wetting theory. On the other hand, such solid PS_{60}-*b*-$PHEMA_{150}$ nanopatterns exhibit extremely robust in aqueous solution, no swelling and reconstruction. Thus, the entropic "steric-repulsive" mechanism [29] for soft hydrophilic polymer brush, i.e., PEG and polysaccharides, cannot be applied here. In order to explain the anti-fouling property of PS_{60}-*b*-$PHEMA_{150}$ nanopatterns, we need to recall the kinetic process of protein adsorption on surface.

Compared with the cell unit (~ μm), the protein molecule (~ nm) has a 10^3 times smaller size with multilevel hierarchies and behaviors in a much more dynamical relaxation mode during living process such as binding interaction, localization and mobility in transportation. The native protein contains both hydrophobic and hydrophilic parts along the molecular structure and, thus, it tends to adsorb on different surfaces, more pronounced on a hydrophobic surface (i.e., PS, PMMA) than a hydrophilic one (i.e., PHEMA, SiO_2). Usually, the protein molecule first comes into contact with the surface, then reorganizes its native 3D conformation and reorients to increase contact with the surface, and finally spreads on and tightly binds to the surface.[30,31] The

intermediate re-arrangement process usually occurs in a mobile state as the protein samples the surface. The faster the mobile protein molecule, the larger surface area required for protein to settle down. By using the homopolymers PS and PHEMA blends with macro-phase separated features, we demonstrated that the area of adhesive pad to attract protein must be more than 2 orders of magnitude larger than the level of contact with surface, or "footprint", of the protein molecule before irreversible adsorption occurs.[32] As for the proteins lysozome (native size in solution, $4.5\times3.0\times3.0$ nm^3), myoglobin ($4.0\times3.5\times2.0$ nm^3), BSA ($14\times4\times4$ nm^3) and fibrinogen ($47\times5\times5$ nm^3) in this work, the threshold size of required adhesive domain have been demonstrated as ~ 100 nm, ~ 100 nm, ~ 600 nm and ~ 2700 nm,[32] respectively, which are much larger than the sticky domelike PS domain (~ 20 nm) on the PS_{60}-*b*-$PHEMA_{150}$ template. Thus, on PS_{60}-*b*-$PHEMA_{150}$, the protein in the mobile precursor state does not have enough space or time to seed on surface for irreversible adsorption before it desorbs from the surface again. In this case, PS_{60}-*b*-$PHEMA_{150}$ nano-patterns with ~ 20 nm dimensions provide repulsive environment for proteins. PS_{140}-*b*-$PHEMA_{150}$ and PS_{200}-*b*-$PHEMA_{50}$ surfaces, by providing larger hydrophobic PS area for the mobile proteins to settle down, are attractive to protein molecules. Recently, we have directly measured surface diffusion coefficient of such mobile state on PS_{60}-*b*-$PHEMA_{150}$ using the total internal reflection fluorescence (TIRF) microscope in the single molecule tracking mode.[28] The quantitative analysis of the mobile state of different proteins and peptides are continuing, which is certainly beyond the scope of this paper.

Compared with the protein adsorption, the mechanism of cell adhesion remains more unclear at the molecular level because of the heterogeneity of cell surface. But one thing is confirmed that the cell communicates with the substrate mainly through the signal membrane proteins outer the cell surface.[22] The repulsive forces between membrane proteins and PS_{60}-*b*-$PHEMA_{150}$ nanopatterns make the PS_{60}-*b*-$PHEMA_{150}$ surface strongly stealth-like to cell adhesion. On the

other hand, neat PS surface is very sticky to membrane proteins and such strong hydrophobic interaction attracts cells, ultimately resulting in the stretched and spread cells on the substrate.

Conclusion

In summary, we have demonstrated a unique heterogeneous nanopattern down to 20 nm scale for highly resistance to the protein adsorption and cell adhesion by using PS_{60}-*b*-$PHEMA_{150}$. PS_{60}-*b*-$PHEMA_{150}$ films with well-ordered patterns were selected because such nanopatterns can not only maintain anti-fouling property but also provide protein-sized nanodomains. These nanopatterns can be utilized to immobilize proteins with nanometer dimensional control. By this way, the reduced sensitivity of protein microarray chips from the clustering or aggregation of immobilized proteins reported in most previous methods can be enhanced. As an ongoing research project, we are trying to interrogate the protein-surface and cell-surface interactions at the molecular level by using PS_{60}-*b*-$PHEMA_{150}$ protein nanoarray chips. We believe that such anti-biofouling nanopatterns may find large variety of applications in nanobiotechnology for fabricating the biosensor arrays and medical devices.

Acknowledgments

This work was supported by National Natural Science Foundation of China (21404046) and Fundamental Research Founds for the Central Universities (HUST: 2014NQ104). We thank the HUST Analytical and Testing Center for allowing us using the facilities.

Figures:

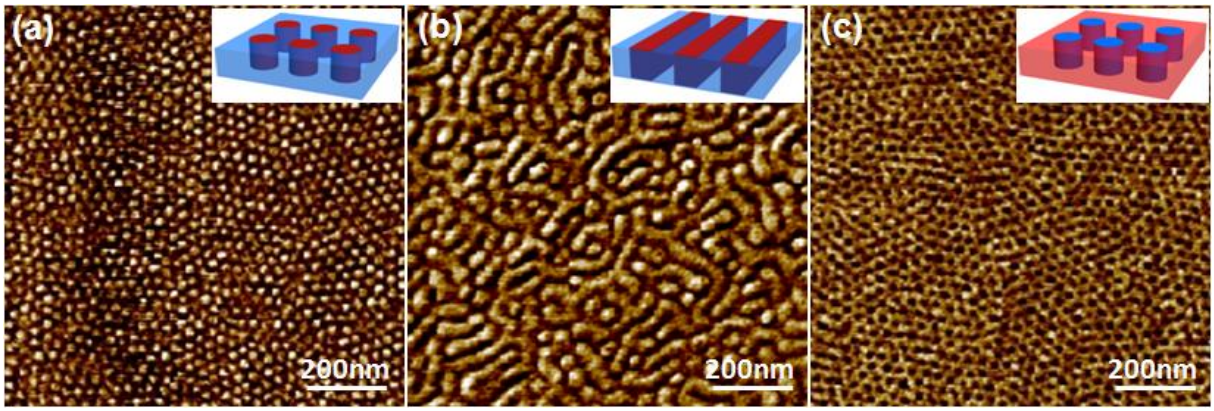

Figure 1. AFM phase images for thin films of (a) PS_{60}-*b*-$PHEMA_{150}$, (b) PS_{140}-*b*-$PHEMA_{150}$ and (c) PS_{200}-*b*-$PHEMA_{50}$ diblock copolymers. The bright area is PS and dark area is PHEMA. Insets in the upper right of images are the cartoons showing the surface morphology of the BCP films where red and blue areas represent the PS and PHEMA domains, respectively.

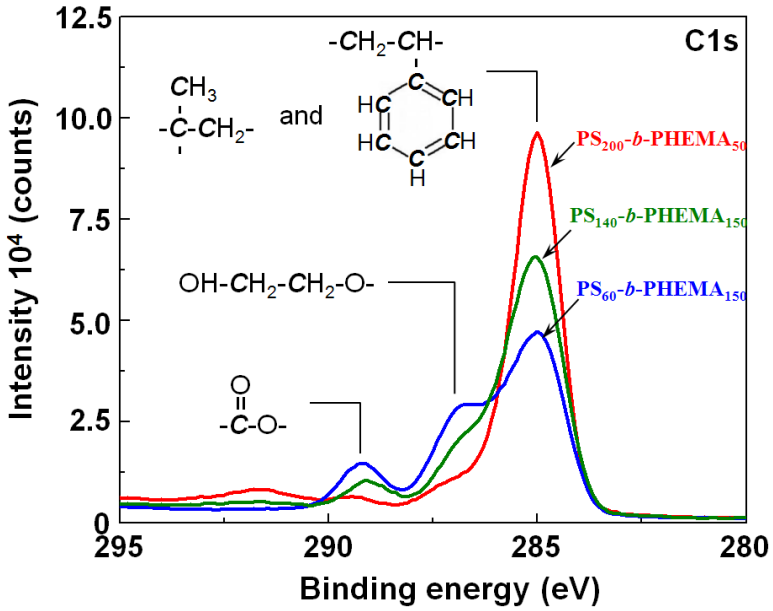

Figure 2. High resolution X-ray photoelectron C 1s spectra for PS_{60}-*b*-$PHEMA_{150}$, PS_{140}-*b*-$PHEMA_{150}$ and PS_{200}-*b*-$PHEMA_{50}$ diblock copolymers thin films.

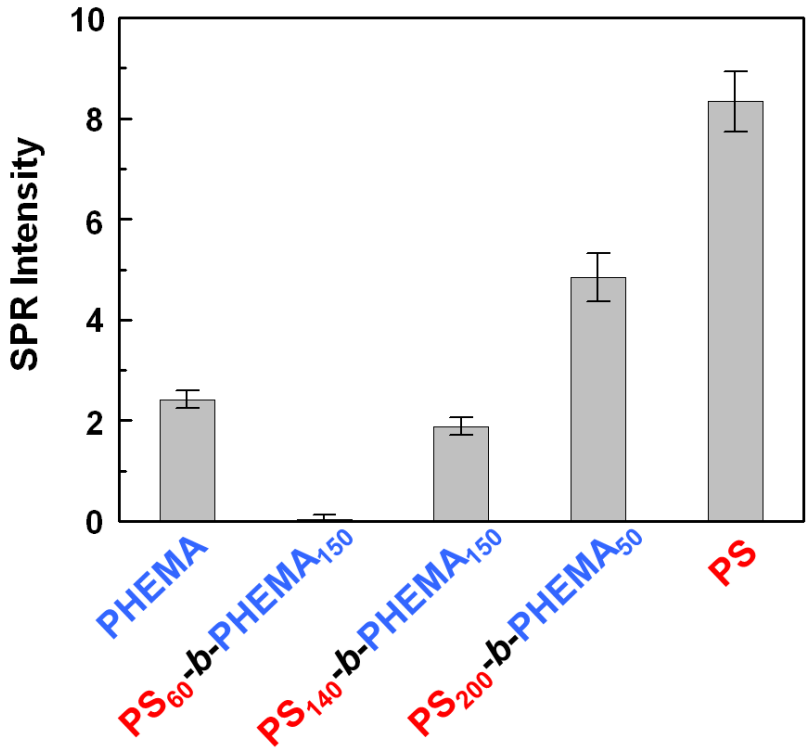

Figure 3. The nonspecific adsorption of lysozome on five different polymer surfaces, PS_{60}-*b*-$PHEMA_{150}$ (PS cylinders in PHEMA matrix), PS_{140}-*b*-$PHEMA_{150}$ (PS/PHEMA lamella structure), PS_{200}-*b*-$PHEMA_{50}$ (PHEMA cylinders in PS matrix), $PHEMA_{7700}$ and PS_{200} homogeneous surfaces.

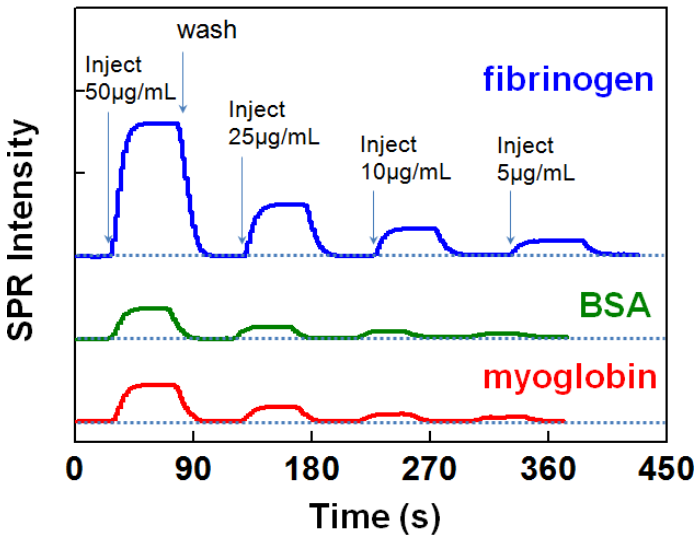

Figure 4. The SPR response for fibrinogen, BSA and myoglobin adsorption on PS_{60}-*b*-$PHEMA_{150}$ nanopattern with PS cylinders in PHEMA matrix at four different protein concentrations: 50, 25, 10, 5 μg/mL.

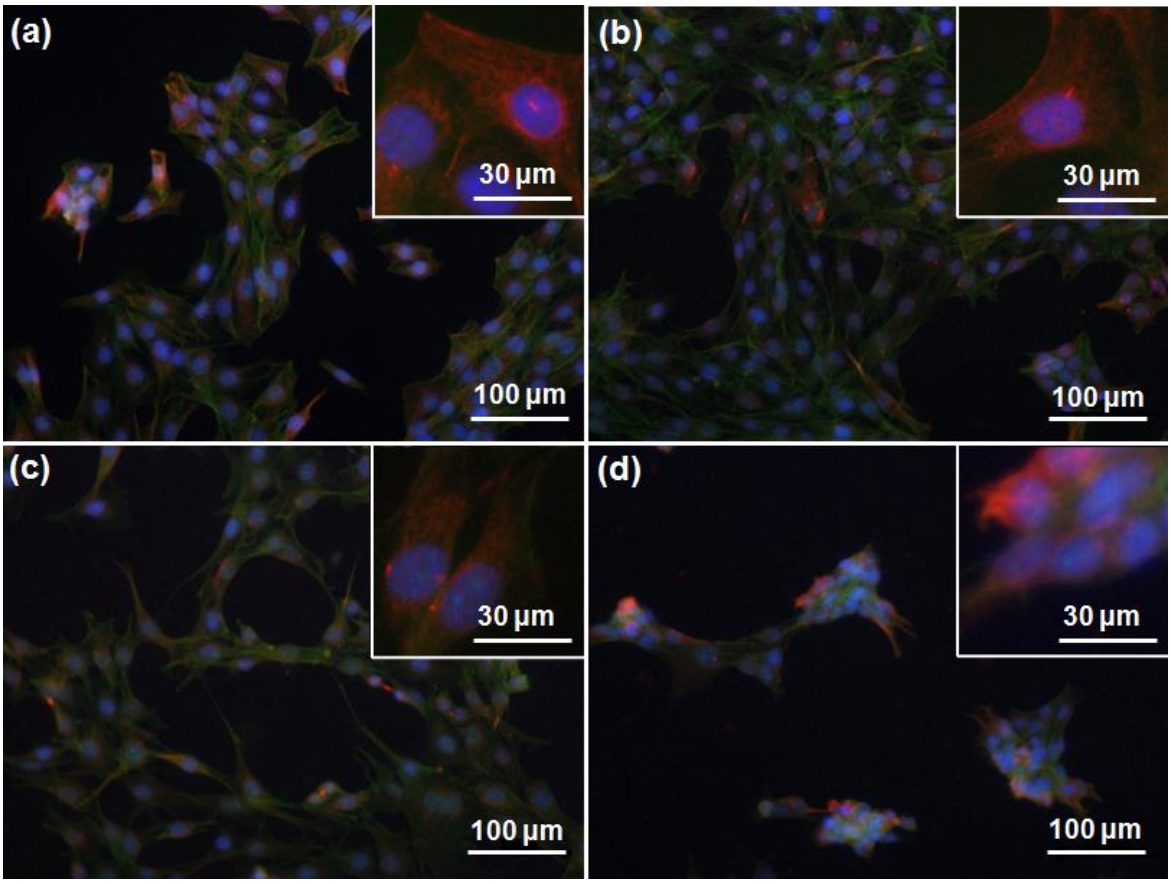

Figure 5. FM images of murine fibroblasts cells NIH-3T3 growing on (a) PS, (b) PS_{200}-*b*-$PHEMA_{50}$, (c) PS_{140}-*b*-$PHEMA_{150}$ and (d) PS_{60}-*b*-$PHEMA_{150}$ after incubation for 24 hrs. Inset in the upper right are FM images at higher magnification.

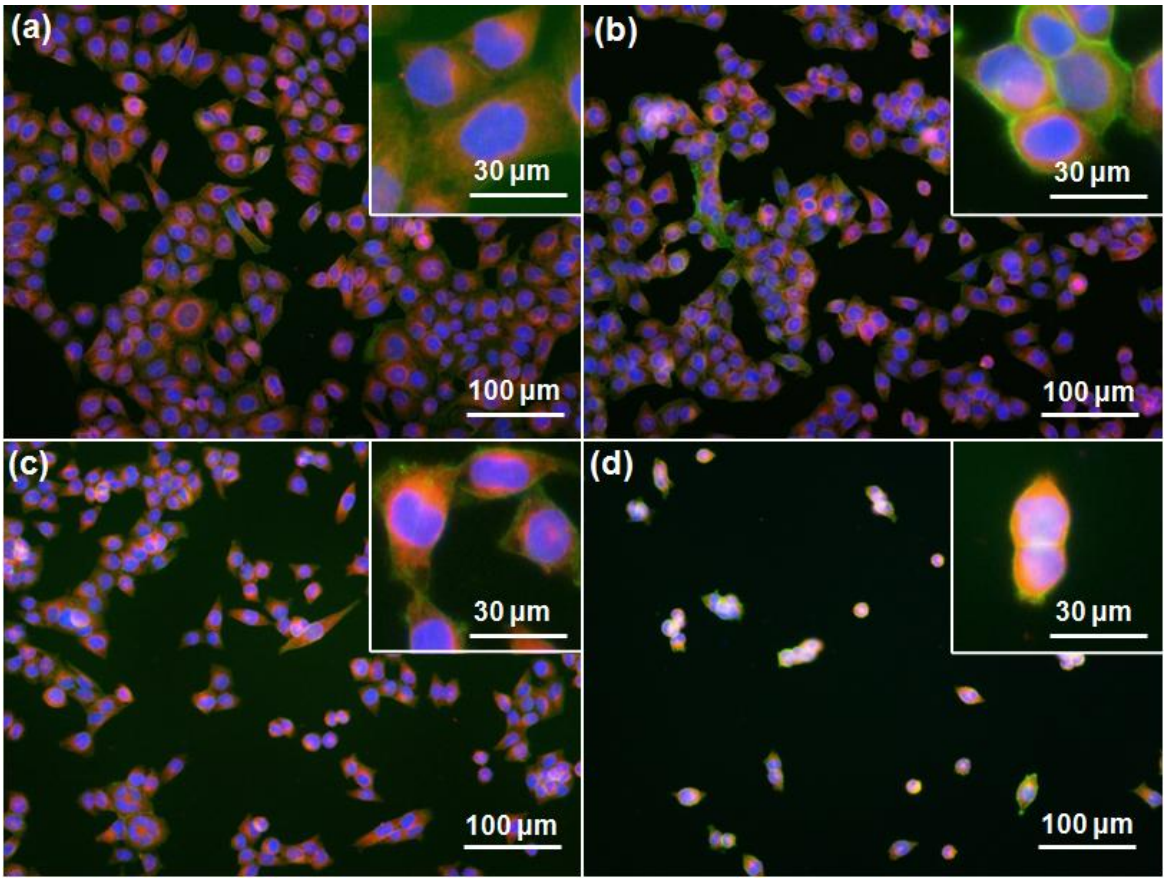

Figure 6. FM images of human prostate carcinoma DU145 growing on (a) PS, (b) PS_{200}-*b*-$PHEMA_{50}$, (c) PS_{140}-*b*-$PHEMA_{150}$ and (d) PS_{60}-*b*-$PHEMA_{150}$ after incubation for 24 hrs. Inset in the upper right are FM images at higher magnification.

References:

(1) J. Vörös, T. Blättler and M. Textor, *MRS Bulletin* 2005, **30**, 202-206.

(2) F. S. Bates and G. H.Fredrickson, *Annu. Rev. Phys. Chem.* 1990, **41**, 525-557.

(3) C. J. Hawker and T. P. Russell, *MRS Bulletin* 2005, **30**, 952-966.

(4) N. Kumar and J. Hahm, *Langmuir* 2005, **21**, 6652-6655.

(5) K. H. A. Lau, J. Bang, D. H. Kim and W. Knoll, *Adv. Funct. Mater.* 2008, **18**, 3148-3157.

(6) N. Kumar, O. Parajuli and J. Hahm, *J. Phys. Chem. B* 2007, **111**, 4581-4587.

(7) C. M. Grozea, N. Gunari, J. A. Finlay, D. Grozea, M. E. Callow, J. A. Callow, Z. H. Lu and G. C. Walker, *Biomacromolecules* 2009, **10**, 1004-1012.

(8) D. Liu, T. Wang and J. L. Keddie, *Langmuir* 2009, **25**, 4526-4534.

(9) E. Martinelli, S. Agostini, G. Galli, E. Chiellini, A. Glisenti, M. E. Pettitt, M. E. Callow, J. A. Callow, K. Graf and F. W. Bartels, *Langmuir* 2008, **24**, 13138-13147.

(10) K. L. Killops, N. Gupta, M. D. Dimitriou, N. A. Lynd, H. Jung, H. Tran, J. Bang, L. M. Campos, *ACS Macro. Lett.* 2012, **1**, 758-763.

(11) J. Hahm, *Langmuir* 2014, **30**, 9891-9904.

(12) W. Norde, *Adv. Colloid & Interface Sci.* 1986, **25**, 267-340.

(13) L. Li, A. P. Hitchcock, N. Robar, R. Cornelius, J. L. Brash, A. Scholl and A. Doran, *J. Phys. Chem. B* 2006, **110**, 16763-16773.

(14) Z. Wu, H. Chen, X. Liu, Y. Zhang, D. Li, and H. Huang, *Langmuir* 2009, **25**, 2900-2906.

(15) T. Okano, S. Nishiyama, I. Shinohara, T. Akaike, Y. Sakurai, K. Kataoka and T. Tsuruta, *J. Biomed. Mater. Res.* 1981, **15**, 393-402.

(16) J. V. M. Weaver, I. Bannister, K. L. Robinson, X. Bories-Azeau, S. P. Armes, M. Smallridge and P. McKenna, *Macromolecules* 2004, **37**, 2395-2403.

(17) F. J. Holly and M. F. Refojo, *J. Biomed. Mater. Res.* 1975, **9**, 315-326.

(18) J. Bang, B. J. Kim, G. E. Stein, T. P. Russell, X. Li, J. Wang, E. J. Kramer and C. J. Hawker, *Macromolecules* 2007, **40**, 7019-7026.

(19) M. S. Lord, M. H. Stenzel, A. Simmons, and B. K. Milthorpe, *Biomaterials* 2006, **27**, 567-575.

(20) D. Leckband, S. Sheth and A. Halperin, *J. Biomater. Sci., Polym. Ed.* 1999, **10**, 1125-1130.

(21) A. G. Gristina, *Science* 1987, **237**, 1588-1595.

(22) E. A. Dubiel, Y. Martin and P. Vermette, *Chem. Rev.* 2011, **111**, 2900-2936.

(23) A. Yayon, M. Klagsbrun, J. D. Esko, P. Leder, and D. M. Ornitz, *Cell* 1991, **64**, 841-848.

(24) P. Majumdar, S. J. Stafslien, J. W. Daniels and D. C. Webster, *J. Coat. Technol. Res.* 2007, **4**, 131-138.

(25) J. A. Finlay, S. Krishnan, M. E. Callow, J. A. Callow, R. Dong, N. Asgill, K. Wong, E. J. Kramer and C. K. Ober, *Langmuir* 2008, **24**, 503-510.

(26) C. S. Gudipati, J. A. Finlay, J. A. Callow, M. E. Callow and K. L. Wooley, *Langmuir* 2005, **21**, 3044-3053.

(27) S. Bhatt, J. Pulpytel, G. Ceccone, P. Lisboa, F. Rossi, V. Kumar and F. Arefi-Khonsari, *Langmuir* 2011, **27**, 14570-14580.

(28) L. Shen, T. Adachi, D. Vanden-Bout and X. Y. Zhu, *J. Am. Chem. Soc.* 2012, **134**, 14172-14178.

(29) S. I. Jeon, J. H. Lee, J. D. Andrade and P. G. de Gennes, *J. Colloid Interface Sci.* 1991, **142**, 149-158.

(30) R. D. Tilton, *Biopolymers at Interfaces.* New York, 1998 edition.

(31) R. D. Tilton, C. D. Robertson and A. P. Gast, *Biophy. J.* 1990, **58**, 1321-1326.

(32) L. Shen and X. Y. Zhu, *Langmuir* 2011, **27**, 7059-7064.

The table of contents entry (TOC):

Title: Anti-biofouling Surface with Sub-20 nm Heterogeneous Nanopatterns

Authors: Lei Shen*, Jun Xie, Juan Tao* and Jintao Zhu*

TOC figure:

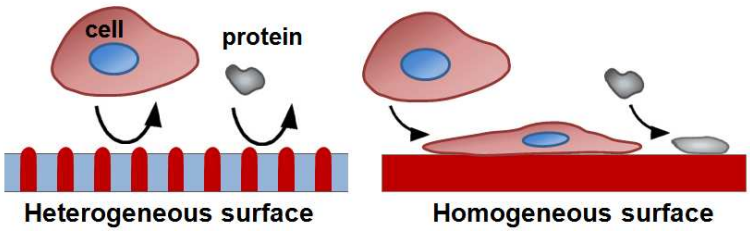

We develop a nanometer-sized heterogeneous pattern with an excellent anti-biofouling property to control over the protein/cell-surface interactions at the molecular level.